Radar Target Detection and Localization Aided by an Active Reconfigurable Intelligent Surface

Emanuele Grossi, *Senior Member, IEEE*, Hedieh Taremizadeh, and Luca Venturino, *Senior Member, IEEE*

***Abstract*—In this letter, we consider a monostatic radar and study the joint detection and localization of a prospective target when the receiver is assisted by a reconfigurable intelligent surface (RIS). To mitigate the multiplicative path loss in the target-RIS-radar hops, we resort to an active RIS, which allows both redirecting and amplifying the incident signal. Upon choosing the array gain factor of the radar transmitter and the RIS to uniformly cover the inspected region, the joint target detection and localization is formulated as a composite hypothesis testing problem, which is solved via a generalized likelihood ratio test (GLRT). Numerical examples are provided to show the merits of the proposed architecture.**

***Index Terms*—Detection, generalized likelihood ratio test, localization, radar, reconfigurable intelligent surfaces.**

I. Introduction

RECONFIGURABLE intelligent surfaces (RISs) are made of tunable elements that reflect the incident electromagnetic signal with a desired phase/amplitude adjustment without using a radio-frequency (RF) chain or introducing a processing delay. RISs can be either passive [1], [2], [3], [4], [5] or active [6], [7], [8] and allow to control the propagation channel from a source to a destination, thus providing additional degrees of freedom in the design of wireless systems [9], [10]; for example, they can be used to overcome the direct-path blockage or to boost the signal-to-noise ratio (SNR) when a direct-path is present [11].

Passive RISs have been exploited in several applications, including joint wireless data and power transfer [12], interference mitigation [13], RIS-based modulation [14], ambient backscatter communication [15], user localization and mapping [16], and radar target detection [17], [18], [19], [20]. Since the source-RIS-destination link suffers from a multiplicative path loss, passive RISs can be of limited help if not properly positioned. A main finding is that they should be better placed close to the source or the destination; however, this may prevent exploiting spatial diversity or may not be feasible due to implementation constraints. These limitations can be overcome by resorting to active RISs, which inherit the same hardware structure and full-duplex operation of the passive counterpart, except that active (rather than passive) load impedances are employed to cover longer source-RIS and/or RIS-destination hops [6], [7], [8], [21]. Active RISs make use of reflection amplifiers, wherein the additional DC power provided by a biasing source is exploited to boost the RF impinging signal [22], [23], [24], [25]; remarkably, tunnel diode based reflection amplifiers only have a sub-mW DC power consumption. An active RIS is somehow similar a network-controlled repeater (NCR), as both devices rely upon the amplify-and-forward concept [26], [27]: however, their different architectures pose unique challenges. Indeed, the RIS employs a single panel with amplifying and reflecting elements, whereby both the impinging and reflected waves must be in the same half-space [6], [8]. On the other hand, the NCR is made of two back-to-back analog arrays with a signal amplifier in between, whereby limiting the loop-back interference in a full-duplex operation may heavily constrain the reciprocal orientation of the two panels [28], [29].

Leveraging the architecture proposed in [21], in this study we consider a monostatic radar that is equipped with a digital array and whose receiver is assisted by a widely-spaced active RIS. The radar illuminates a given area and, in the presence of a target, receives two independent echoes, namely, the direct and the RIS-assisted (indirect) echo: this system mimics a distributed multi-static radar; however, rather than having a second receiver with an additional RF processing chain, the RIS redirects the indirect echo towards the same receiver observing the direct echo. While [21] has only focused on target detection, our goal here is to configure the RIS and elaborate the received signal to jointly detect and localize a prospective target; in addition, we remove the assumption that the radar receiver has two separate antennas pointing towards the target and the RIS, respectively. Upon introducing a convenient signal model, we design the array gain factor of the radar transmitter and the RIS to uniformly cover the inspected region; then, the joint detection and localization problem is solved through a generalized likelihood ratio test (GLRT). Numerical examples are provided to assess the achievable performance and to elicit the impact of the RIS amplification gain and of the size of the inspected region.

The remainder of this work is organized as follows. Section II contains the system description.[1] Section III illustrates the proposed system design. Section IV contains the numerical analysis. Finally, concluding remarks are given in Section V.

Manuscript received 26 April 2023; revised 7 June 2023; accepted 14 July 2023. Date of publication 17 July 2023; date of current version 26 July 2023. This work was supported by the Italian Ministry of University and Research through the grants Dipartimenti di Eccellenza 2018–2022 and PRIN 2022. The associate editor coordinating the review of this manuscript and approving it for publication was Prof. Zhiguo Shi. *(Corresponding author: Luca Venturino.)*

Emanuele Grossi and Luca Venturino are with the Department of Electrical and Information Engineering, University of Cassino and Southern Lazio, 03043 Cassino, Italy, and also with the CNIT, 43124 Parma, Italy (e-mail: e.grossi@unicas.it; l.venturino@unicas.it).

Hedieh Taremizadeh is with the Department of Electrical and Information Engineering, University of Cassino and Southern Lazio, 03043 Cassino, Italy (e-mail: hedieh.taremizadeh@unicas.it).

Digital Object Identifier 10.1109/LSP.2023.3296372

[1] Column vectors/matrices are denoted by lower/uppercase boldface letters. The symbols $\Re\{\cdot\}$, $(\cdot)^*$, $(\cdot)^{\mathsf{T}}$, $(\cdot)^{\mathsf{H}}$, $\star$, and $\otimes$ denotes real part, conjugate, transpose, conjugate-transpose, convolution, and Kronecker product, respectively. $\mathbb{C}$ is the set of complex numbers. $\boldsymbol{I}_M$ is the $M \times M$ identity matrix. $\mathrm{diag}\{\boldsymbol{x}\}$ is a diagonal matrix with the elements of $\boldsymbol{x}$ on the main diagonal.

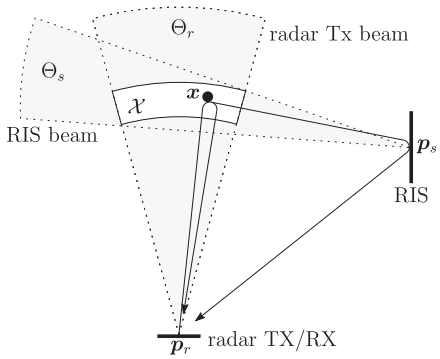

Fig. 1. Considered architecture composed of a monostatic radar and an active RIS assisting the receiver.

II. System Description

We consider a monostatic radar that employs a carrier wavelength λ, an average radiated power $\mathcal{P}_r$, a pulse repetition time T_r, and a uniform linear array with N_r elements spaced of δ_r. For simplicity, we assume a two-dimensional geometry, as shown in Fig. 1. The radar transmitter emits the baseband signal $\sqrt{\mathcal{P}_r T_r}\phi_r(t)\boldsymbol{b}_r^*$, where $\boldsymbol{b}_r \in \mathbb{C}^{N_r}$ is a unit-norm spatial beamformer and $\phi_r(t)$ is a unit-energy pulse with support $[0, \Phi_r]$ and bandwidth W_r. The radar receiver is assisted by an active RIS containing N_s elements arranged into a uniform square array with inter-element spacing δ_s along each axis. We denote by $\sqrt{B_s}\boldsymbol{b}_s^* \in \mathbb{C}^{N_s}$ the RIS response, where $\|\boldsymbol{b}_s\|^2 = N_s$ and B_s is the average element gain. The inspected region $\mathcal{X} \subset \mathbb{R}^2$ is in the radar and RIS far-field; also, radar and RIS are in each other's far-field and sufficiently spaced to provide independent looks at a prospective target in $\mathcal{X}$ [21].

In the following, $\mathcal{H}$ and $\bar{\mathcal{H}}$ denote the null hypothesis (i.e., no target is present) and its alternative (i.e., one target is present at an unknown location $\boldsymbol{x} \in \mathcal{X}$), respectively. Also, $\boldsymbol{p}_r \in \mathbb{R}^2$ is the position of the radar phase center; $d_r(\boldsymbol{p}) \geq 0$ and $\theta_r(\boldsymbol{p}) \in (-\pi/2, \pi/2)$ are the distance and angle of a point $\boldsymbol{p} \in \mathbb{R}^2$ with respect to the radar phase center, respectively; $\Theta_r \subset (-\pi/2, \pi/2)$ is the angular sector containing the inspected region, as seen from the radar phase center; $\boldsymbol{u}_r(\theta) \in \mathbb{C}^{N_r}$ and $G_r(\theta) \geq 0$ are the array manifold vector and the element gain of the radar towards the angular direction $\theta \in (-\pi/2, \pi/2)$, respectively. For the RIS, $\boldsymbol{p}_s$, $d_s(\boldsymbol{p})$, $\theta_s(\boldsymbol{p})$, Θ_s, $\boldsymbol{u}_s(\theta)$, and $G_s(\theta)$ are similarly defined. Finally, $\Gamma_r(\theta) = \left|\boldsymbol{b}_r^{\mathsf{H}}\boldsymbol{u}_r(\theta)\right|^2$ and $\Gamma_s(\theta) = \left|\boldsymbol{b}_s^{\mathsf{H}}\mathrm{diag}\{\boldsymbol{u}_s(\theta_s(\boldsymbol{p}_r))\}\boldsymbol{u}_s(\theta)\right|^2$ are the array gain factors of the radar transmitter and the RIS, respectively, with $\theta \in (-\pi/2, \pi/2)$.

We assume that the RIS does not obstruct the radar view, i.e., $\theta_r(\boldsymbol{p}_s) \notin \Theta_r$, and that the RIS is not illuminated by the radar transmitter, i.e., $\Gamma_r(\theta_r(\boldsymbol{p}_s)) \simeq 0$ (more on this in Section III). Under $\bar{\mathcal{H}}$, the target scatters part of the incident signal back towards the radar receiver (direct echo) and part towards the RIS that in turn amplifies and redirects it towards the radar receiver (indirect echo); accordingly, the received signal is

$$\boldsymbol{y}(t) = \begin{cases} \alpha_1(\boldsymbol{x})\boldsymbol{h}_1(t;\boldsymbol{x}) + \alpha_2(\boldsymbol{x})\boldsymbol{h}_2(t;\boldsymbol{x}) + \boldsymbol{n}(t), & \text{under } \bar{\mathcal{H}} \\ \boldsymbol{n}(t), & \text{under } \mathcal{H} \end{cases} \tag{1}$$

where $\boldsymbol{h}_1(t;\boldsymbol{x}) \in \mathbb{C}^{N_r}$ and $\boldsymbol{h}_2(t;\boldsymbol{x}) \in \mathbb{C}^{N_r}$ are the space-time signatures of the direct and indirect echoes under $\bar{\mathcal{H}}$, respectively, $\alpha_1(\boldsymbol{x}) \in \mathbb{C}$ and $\alpha_2(\boldsymbol{x}) \in \mathbb{C}$ are the corresponding amplitudes, and $\boldsymbol{n}(t) \in \mathbb{C}^{N_r}$ is the Gaussian noise. Assuming a narrowband signal [30], we have $\boldsymbol{h}_1(t;\boldsymbol{x}) = \boldsymbol{u}_r(\theta_r(\boldsymbol{x}))\phi_r(t - \tau_1(\boldsymbol{x}))$ and $\boldsymbol{h}_2(t;\boldsymbol{x}) = \boldsymbol{u}_r(\theta_r(\boldsymbol{p}_s))\phi_r(t - \tau_2(\boldsymbol{x}))$, where $\tau_1(\boldsymbol{x}) = 2d_r(\boldsymbol{x})/c$, $\tau_2(\boldsymbol{x}) = (d_r(\boldsymbol{x}) + d_s(\boldsymbol{x}) + d_r(\boldsymbol{p}_s))/c$, and c is the speed of light. Also, assuming a free-space propagation [31], we have $\alpha_1(\boldsymbol{x}) = \gamma_1(\boldsymbol{x})\tilde{\alpha}_1$, where $\tilde{\alpha}_1 \in \mathbb{C}$ is the unknown (monostatic) target response, while

$$\gamma_1^2(\boldsymbol{x}) = \underbrace{\mathcal{P}_r T_r}_{\substack{\text{radiated} \\ \text{energy}}} \underbrace{\Gamma_r\left(\theta_r(\boldsymbol{x})\right)}_{\substack{\text{transmit} \\ \text{array gain}}} \underbrace{\frac{G_r\left(\theta_r(\boldsymbol{x})\right)}{4\pi d_r^2(\boldsymbol{x})}}_{\substack{\text{link budget in the} \\ \text{radar-target hop}}} \underbrace{\frac{G_r\left(\theta_r(\boldsymbol{x})\right)\lambda^2}{(4\pi)^2 d_r^2(\boldsymbol{x})}}_{\substack{\text{link budget in the} \\ \text{target-radar hop}}}. \tag{2}$$

Similarly, $\alpha_2(\boldsymbol{x}) = \gamma_2(\boldsymbol{x})\tilde{\alpha}_2$, where $\tilde{\alpha}_2 \in \mathbb{C}$ is the unknown (bistatic) target response and

$$\gamma_2^2(\boldsymbol{x}) = \underbrace{\mathcal{P}_r T_r}_{\substack{\text{radiated} \\ \text{energy}}} \underbrace{\Gamma_r\left(\theta_r(\boldsymbol{x})\right)}_{\substack{\text{transmit} \\ \text{array gain}}} \underbrace{\frac{G_r(\theta_r(\boldsymbol{x}))}{4\pi d_r^2(\boldsymbol{x})}}_{\substack{\text{link budget in the} \\ \text{radar-target hop}}} \underbrace{\frac{G_s(\theta_s(\boldsymbol{x}))\lambda^2}{(4\pi)^2 d_s^2(\boldsymbol{x})}}_{\substack{\text{link budget in the} \\ \text{target-RIS hop}}}$$
$$\times \underbrace{\Gamma_s\left(\theta_s(\boldsymbol{x})\right)}_{\substack{\text{RIS} \\ \text{array gain}}} \underbrace{\frac{B_s G_s(\theta_s(\boldsymbol{p}_r))\, G_r\left(\theta_r(\boldsymbol{p}_s)\right)\lambda^2}{(4\pi)^2 d_r^2(\boldsymbol{p}_s)}}_{\text{link budget in the RIS-radar hop}}. \tag{3}$$

Following [6], [7], [8], [21], the noise is the sum of two independent contributions, namely, $\boldsymbol{n}(t) = \boldsymbol{n}_r(t) + n_s(t)\boldsymbol{u}_r(\theta_r(\boldsymbol{p}_s))$. Here, $\boldsymbol{n}_r(t)$ is the noise of the radar receiver, and its entries are modeled as independent white Gaussian processes with power spectral density (PSD) $\sigma_{r,n}^2$. Instead, $n_s(t)$ is the noise coming from the RIS that is amplified together with the signal of interest and redirected towards the radar receiver; in particular, we have $n_s(t) = g_s\boldsymbol{b}_s^{\mathsf{H}}\mathrm{diag}\{\boldsymbol{u}_s(\theta_s(\boldsymbol{p}_r))\}\tilde{\boldsymbol{n}}_s(t)$, where

$$g_s = \left(\frac{B_s G_s\left(\theta_s(\boldsymbol{p}_r)\right) G_r\left(\theta_r(\boldsymbol{p}_s)\right)\lambda^2}{(4\pi)^2 d_r^2(\boldsymbol{p}_s)}\right)^{1/2} \tag{4}$$

while the n-th entry of $\tilde{\boldsymbol{n}}_s(t) \in \mathbb{C}^{N_s}$ is the dynamic noise of the n-th RIS element, accounting for both the input and the internal noise, assumed independent of the reflected signal. The entries of $\tilde{\boldsymbol{n}}_s(t)$ are modeled as independent white Gaussian processes with PSD $\sigma_{s,\tilde{n}}^2$, so that $n_s(t)$ is itself a white Gaussian process with PSD $\sigma_{s,n}^2 = g_s^2\|\boldsymbol{b}_s\|^2\sigma_{s,\tilde{n}}^2$. We assume that both $\sigma_{r,n}^2$ and $\sigma_{s,n}^2$ are known; for example, they can be estimated by resorting to secondary data.

Finally, the power consumed by the radar transmitter can be modeled as $\mathcal{P}_r^{\text{tot}} = \rho_r + \eta_{r,\text{all}}^{-1}\mathcal{P}_r$, where ρ_r is the static power [32] and $\eta_{r,\text{all}}$ is the overall efficiency of the RF amplifier [33, Eq. (10)]. Instead, the power consumed by the active RIS can be modeled as $\mathcal{P}_s^{\text{tot}} = \left(\rho_s + \eta_{s,\text{PAE}}^{-1}\mathcal{P}_{s,in}(B_s - 1)\right)N_s$, where $\rho_s = \rho_{s,c} + \rho_{s,dc}$ is the static power per each element [6], [24], with $\rho_{s,c}$ being the switch and control circuit power and $\rho_{s,dc}$ the DC biasing power, $\eta_{s,\text{PAE}}$ is the power-added efficiency (PAE) of the amplifier [33, Eq. (12)],

$$\mathcal{P}_{s,in} = \sigma_{s,\tilde{n}}^2 W_r + \mathcal{P}_r\Gamma_r\left(\theta_r(\boldsymbol{x})\right)\frac{G_r\left(\theta_r(\boldsymbol{x})\right)}{4\pi d_r^2(\boldsymbol{x})}\frac{G_s\left(\theta_s(\boldsymbol{x})\right)\lambda^2}{(4\pi)^2 d_s^2(\boldsymbol{x})}|\tilde{\alpha}_2|^2 \tag{5}$$

is the input power (i.e., the sum of the dynamic noise power and incident power), and $\mathcal{P}_{s,in}(B_s-1)$ is the difference between the output and input power; the term $\eta_{s,\text{PAE}}^{-1}\mathcal{P}_{s,in}(B_s-1)$ is often much smaller than $\rho_{s,dc}$. Notice that $\mathcal{P}_s^{\text{tot}}=N_s\rho_{s,c}$ for a passive RIS and $\mathcal{P}_s^{\text{tot}}=0$ if no RIS is present. Hence, for the same power budget[2] $\mathcal{P}^{\text{tot}}=\mathcal{P}_r^{\text{tot}}+\mathcal{P}_s^{\text{tot}}$, the radar radiates more power when a passive RIS or no RIS is employed.

III. System Design

In this section, we first illustrate the design of the radar transmitter and RIS; then, we consider the radar receiver.

Given the prior uncertainty on the target location, we propose to choose $\boldsymbol{b}_r$ and $\boldsymbol{b}_s$ so that $\Gamma_r(\theta)$ and $\Gamma_s(\theta)$ approximate an ideal rectangular function that is non-zero only if $\theta\in\Theta_r$ and $\theta\in\Theta_s$, respectively, so as to ensure a uniform converge of the inspected region. Many matching criteria are available in the literature: see [30] and references therein. For example, in Section IV we resort to a least-square solution with a Taylor tapering to reduce the level of the sidelobes.

The received signal $\boldsymbol{y}(t)$ is sent to a low-pass filter with impulse response $\psi_r(t)=\sqrt{\Psi_r}\,\text{Rect}(t/\Psi_r)$, where $\text{Rect}(t)$ is a unit-amplitude rectangular pulse with support [0,1] and $1/\Psi_r\geq W_r$; the filter output is then sampled at rate $1/\Psi_r$ in the time interval $[\tau_{\min},\tau_{\max}+\Phi_r+\Psi_r]$, where $\tau_{\min}=\min_{i\in\{1,2\},\,\boldsymbol{x}\in\mathcal{X}}\tau_i(\boldsymbol{x})$ and $\tau_{\max}=\max_{i\in\{1,2\},\,\boldsymbol{x}\in\mathcal{X}}\tau_i(\boldsymbol{x})$. The samples taken at the time epochs $\{\tau_{\min}+\ell\Psi_r\}_{\ell=0}^{F_r-1}$ are organized into a vector $\boldsymbol{y}\in\mathbb{C}^{M_r}$, where $F_r=\lfloor(\tau_{\max}-\tau_{\min}+\Phi_r+\Psi_r)/\Psi_r\rfloor+1$ and $M_r=N_rF_r$. Let $\boldsymbol{\phi}_{r,i}(\boldsymbol{x})\in\mathbb{C}^{F_r}$ be the vector containing the samples of the filtered waveform $\phi_r(t-\tau_i(\boldsymbol{x}))\star\psi_r(t)$, for $i=1,2$; then, we have

$$\boldsymbol{y}=\begin{cases}\boldsymbol{H}(\boldsymbol{x})\boldsymbol{\alpha}(\boldsymbol{x})+\boldsymbol{n}, & \text{under }\bar{\mathcal{H}}\\ \boldsymbol{n}, & \text{under }\mathcal{H}\end{cases}\tag{6}$$

where $\boldsymbol{\alpha}(\boldsymbol{x})=[\alpha_1(\boldsymbol{x})\;\alpha_2(\boldsymbol{x})]^{\mathsf{T}}$, $\boldsymbol{H}(\boldsymbol{x})=[\boldsymbol{h}_1(\boldsymbol{x})\;\boldsymbol{h}_2(\boldsymbol{x})]$, $\boldsymbol{h}_1(\boldsymbol{x})=\boldsymbol{u}_r(\theta_r(\boldsymbol{x}))\otimes\boldsymbol{\phi}_{r,1}(\boldsymbol{x})$, and $\boldsymbol{h}_2(\boldsymbol{x})=\boldsymbol{u}_r(\theta_r(\boldsymbol{p}_s))\otimes\boldsymbol{\phi}_{r,2}(\boldsymbol{x})$, while $\boldsymbol{n}$ contains the samples of the filtered noise. Under the considered assumptions, $\boldsymbol{H}(\boldsymbol{x})$ is full column-rank for any $\boldsymbol{x}\in\mathcal{X}$, and $\boldsymbol{n}$ is a circularly-symmetric complex Gaussian vector with covariance matrix $\boldsymbol{C}=(\sigma_{r,n}^2\boldsymbol{I}_{N_r}+\sigma_{s,n}^2\boldsymbol{u}_r(\theta_r(\boldsymbol{p}_s))\boldsymbol{u}_r^{\mathsf{H}}(\theta_r(\boldsymbol{p}_s)))\otimes\boldsymbol{I}_{F_r}$.

We solve the binary test in (6) by resorting to a GLRT, wherein we treat the target location $\boldsymbol{x}$ and the corresponding signal amplitudes $\alpha_1(\boldsymbol{x})$ and $\alpha_2(\boldsymbol{x})$ under $\bar{\mathcal{H}}$ as unknown deterministic parameters [34]. Given $\boldsymbol{x}$ and $\boldsymbol{\alpha}(\boldsymbol{x})$, the log-likelihood ratio between $\bar{\mathcal{H}}$ and $\mathcal{H}$ is

$$\begin{aligned}\Lambda\left(\boldsymbol{x},\boldsymbol{\alpha}(\boldsymbol{x})\right)=2\Re\left\{\boldsymbol{\alpha}^{\mathsf{H}}(\boldsymbol{x})\boldsymbol{H}^{\mathsf{H}}(\boldsymbol{x})\boldsymbol{C}^{-1}\boldsymbol{y}\right\}\\-\boldsymbol{\alpha}^{\mathsf{H}}(\boldsymbol{x})\boldsymbol{H}^{\mathsf{H}}(\boldsymbol{x})\boldsymbol{C}^{-1}\boldsymbol{H}(\boldsymbol{x})\boldsymbol{\alpha}(\boldsymbol{x})\end{aligned}\tag{7}$$

which is maximized when $\boldsymbol{\alpha}(\boldsymbol{x})$ is chosen as

$$\left(\boldsymbol{H}^{\mathsf{H}}(\boldsymbol{x})\boldsymbol{C}^{-1}\boldsymbol{H}(\boldsymbol{x})\right)^{-1}\boldsymbol{H}^{\mathsf{H}}(\boldsymbol{x})\boldsymbol{C}^{-1}\boldsymbol{y}.\tag{8}$$

Accordingly, the GLRT becomes

$$\max_{\boldsymbol{x}\in\mathcal{X}}\left\|\boldsymbol{\Pi}^{\mathsf{H}}(\boldsymbol{x})\boldsymbol{y}\right\|^2\underset{\bar{\mathcal{H}}}{\overset{\mathcal{H}}{\gtrless}}\eta\tag{9}$$

[2]We omit in this power budget the consumption of the radar receiver, which can be assumed to be the same whether or not a help RIS is considered.

where $\boldsymbol{\Pi}(\boldsymbol{x})=\boldsymbol{C}^{-1}\boldsymbol{H}(\boldsymbol{x})(\boldsymbol{H}^{\mathsf{H}}(\boldsymbol{x})\boldsymbol{C}^{-1}\boldsymbol{H}(\boldsymbol{x}))^{-1/2}$ and η is a threshold set to have a specified probability of false alarm (PFA). Notice that $\|\boldsymbol{\Pi}^{\mathsf{H}}(\boldsymbol{x})\boldsymbol{y}\|^2$ is the energy of the whitened observation $\boldsymbol{C}^{-1/2}\boldsymbol{y}$ falling in the two-dimensional column space of $\boldsymbol{C}^{-1/2}\boldsymbol{H}(\boldsymbol{x})$. As customary, the maximization over $\mathcal{X}$ is undertaken by a grid search. If $\mathcal{H}$ is declared, the argument of the maximum provides an estimate of the target location. The following remarks are now in order.

Remark 1: If $\boldsymbol{h}_1^{\mathsf{H}}(\boldsymbol{x})\boldsymbol{C}^{-1}\boldsymbol{h}_2(\boldsymbol{x})=0$, then the k-th column of $\boldsymbol{\Pi}(\boldsymbol{x})$ is simply $\boldsymbol{C}^{-1}\boldsymbol{h}_k(\boldsymbol{x})/(\boldsymbol{h}_k^{\mathsf{H}}(\boldsymbol{x})\boldsymbol{C}^{-1}\boldsymbol{h}_k(\boldsymbol{x}))^{1/2}$. Since

$$\boldsymbol{h}_1^{\mathsf{H}}(\boldsymbol{x})\boldsymbol{C}^{-1}\boldsymbol{h}_2(\boldsymbol{x})=\frac{\boldsymbol{u}_r^{\mathsf{H}}\left(\theta_r(\boldsymbol{x})\right)\boldsymbol{u}_r\left(\theta_r(\boldsymbol{p}_s)\right)\boldsymbol{\phi}_{r,1}^{\mathsf{H}}(\boldsymbol{x})\boldsymbol{\phi}_{r,2}(\boldsymbol{x})}{\sigma_{r,n}^2+N_r\sigma_{s,n}^2}\tag{10}$$

this occurs when the steering vectors towards the prospective target and the RIS are orthogonal or if the delay offset between the direct and indirect echoes exceeds the duration of $\phi_r(t)\star\psi_r(t)$, i.e., $|d_s(\boldsymbol{x})+d_r(\boldsymbol{p}_s)-d_r(\boldsymbol{x})|>c(\Phi_r+\Psi_r)$.

Remark 2: When no RIS is employed, the GLRT has still the form in (9) with $\boldsymbol{\Pi}(\boldsymbol{x})=\boldsymbol{C}^{-1}\boldsymbol{h}_1(\boldsymbol{x})/(\boldsymbol{h}_1^{\mathsf{H}}(\boldsymbol{x})\boldsymbol{C}^{-1}\boldsymbol{h}_1(\boldsymbol{x}))^{1/2}$. Since $\|\boldsymbol{\Pi}^{\mathsf{H}}(\boldsymbol{x})\boldsymbol{y}\|^2$ is now the energy of the whitened observation $\boldsymbol{C}^{-1/2}\boldsymbol{y}$ falling in the one-dimensional subspace spanned by $\boldsymbol{C}^{-1/2}\boldsymbol{h}_1(\boldsymbol{x})$, for a fixed PFA, the GLRT needs here a lower threshold as compared to the proposed case.

Remark 3: The matrices $\{\boldsymbol{\Pi}(\boldsymbol{x})\}_{\boldsymbol{x}\in\mathcal{X}}$ can be computed off-line with a computational complexity that scales quadratically with the length M_r of the observation vector and linearly with the number $|\mathcal{X}|$ of grid points. Instead, given the current measurement $\boldsymbol{y}$, the in-line implementation of the GLRT in (9) is dominated by the multiplication of $\boldsymbol{\Pi}^{\mathsf{H}}(\boldsymbol{x})$ by $\boldsymbol{y}$ for each grid point, so that the computational complexity scales linearly with both M_r and $|\mathcal{X}|$. Interestingly, when no RIS is present, the above asymptotic costs remain the same.

Remark 4: When multiple targets are present in $\mathcal{X}$, we may resort to standard approaches, such as for example subspace-based iterative procedures that extract one target at a time after eliminating the previously-detected signal components [35].

IV. Performance Analysis

We consider an X-band system with $\lambda=3$ cm, $G_r(\theta)=G_s(\theta)=2\cos(\theta)\text{Rect}(\theta/\pi+1/2)$, $T_r=10$ μs, $\phi_r(t)=\sqrt{\Phi_r}\,\text{Rect}(t/\Phi_r)$, $\Phi_r=\Psi_r=0.1$ μs, $W_r=10$ MHz, $N_r=16$, $N_s=3600$, $\delta_r=\delta_s=\lambda/2$, and $\sigma_{r,n}^2=\sigma_{s,\tilde{n}}^2=1.6\cdot10^{-20}$ W/Hz. As to the power consumption, we assume $\rho_r=30$ W, $\eta_{r,\text{all}}=0.9$, and $\mathcal{P}_r=8$ W for the radar transmitter, which gives a system efficiency $\mathcal{P}_r/\mathcal{P}_r^{\text{tot}}$ of about 20%, and $\rho_{s,c}=0.1$ mW, $\rho_{s,dc}=0.32$ mW, and $\eta_{s,\text{PAE}}=0.8$ for the active RIS. As to the target, $\tilde{\alpha}_1$ and $\tilde{\alpha}_2$ are generated as independent realizations of a circularly-symmetric Gaussian random variable with variance σ_t^2. With reference to Fig. 1, the radar is at the origin of the coordinate system and inspects the range interval $[500-\Delta_r/2,500+\Delta_r/2]$ m in the angular sector $\Theta_r=[-5^\circ,5^\circ]$, while the RIS is at (300,300) m. Two values of Δ_r are considered, namely, 15 and 150 m, with the former corresponding to the range resolution $c/(2W_r)$. The top plot in Fig. 2 shows the array gain factor $\Gamma_r(\theta)$ of the radar transmitter; here, the mainbeam covers the angular sector Θ_r, and a null is placed at $\theta=\theta_r(\boldsymbol{p}_s)=\pi/4$. The middle and bottom plots in Fig. 2 show the array gain factor $\Gamma_s(\theta)$ of the RIS for $\Delta_r=15,150$ m, respectively; notice

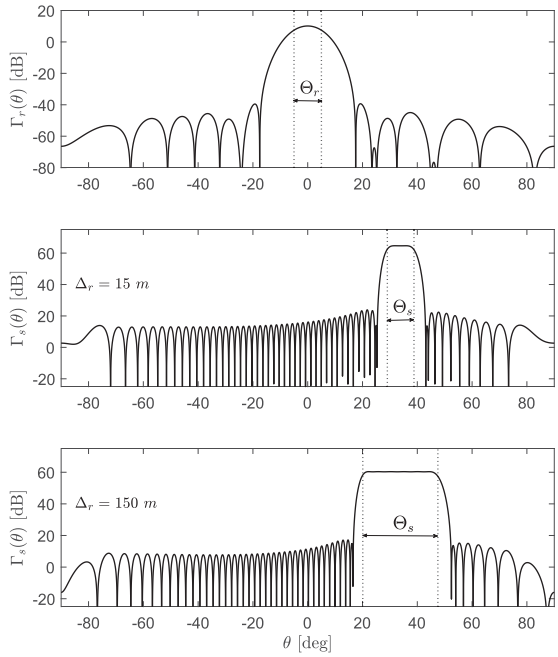

Fig. 2. Top plot: array gain factor of the radar transmitter. Middle and bottom plots: array gain factor of the RIS for $\Delta_r = 15, 150$ m, respectively.

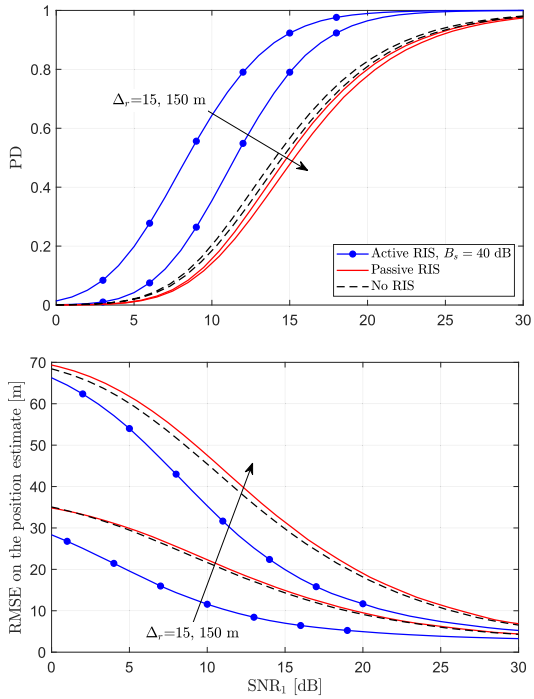

Fig. 3. PD (top plot) and RMSE on the position estimate (bottom plot) versus SNR_1 when $\Delta_r = 15, 150$ m and no RIS, a passive RIS, and an active RIS with $B_s = 40$ dB are employed.

here that a wider mainbeam is required to cover the region of interest when Δ_r increases, at the price of a lower array gain.

We define the SNR of the direct echo as $\text{SNR}_1 = N_r\gamma_1^2(\bar{\boldsymbol{x}})\sigma_t^2/\sigma_{r,n}^2$, where $\bar{\boldsymbol{x}}$ is a reference point with range 500 m and azimuth 0°. Fig. 3 shows the detection probability (PD) and the root mean square error (RMSE) in the target localization of the proposed architecture versus SNR_1 when $B_s = 40$ dB. The reported values are computed over 10^5 independent snapshots, while SNR_1 is varied by increasing the radar target cross-section σ_t^2. In each snapshot, the target is randomly dropped in $\mathcal{X}$ under $\bar{\mathcal{H}}$. The performance of the proposed architecture is contrasted with that of a radar helped by a passive RIS or operating alone, when keeping the same consumed power $\mathcal{P}^{\text{tot}}$; in all cases, the detection threshold is chosen to have $\text{PFA} = 10^{-5}$.

It is seen that helping the radar receiver with an active RIS can improve both the detection and localization performance of an existing radar. Instead, using a passive RIS may be even detrimental in the considered scenario. To explain these results, recall that an RIS-aided system radiates less power to maintain the same power consumption (see Section II), as compared to a radar operating alone; also, the corresponding GLRT presents a larger threshold to maintain the same PFA (see Remark 2); accordingly, processing the indirect echo becomes beneficial only if a signal amplification (in addition to the array gain) is introduced at the RIS to compensate for the multiplicative pathloss along the target-RIS-radar hops. To better illustrate this point, Table I reports the values of PD and RMSE for different amplification gains when $\text{SNR}_1 = 15$ dB, along with the SNR of the indirect echo, defined as $\text{SNR}_2 = N_r\gamma_2^2(\bar{\boldsymbol{x}})\sigma_t^2/(\sigma_{r,n}^2 + \sigma_{s,n}^2)$: it is seen that a help RIS is advantageous only if B_s is sufficiently large to make SNR_2 comparable to or larger than SNR_1. Finally, for the same amplification gain, both Fig. 3 and Table I indicate that the active RIS becomes less rewarding when the inspected region $\mathcal{X}$ is enlarged: this is indeed due to the fact that the RIS array gain decreases, as previously shown in Fig. 2.

TABLE I
PD, RMSE, AND SNR_2 WHEN $\text{SNR}_1 = 15$ dB

Δ_r [m]		No RIS	Passive RIS	Active RIS: B_s [dB]			
				25	30	35	40
15	PD	0.56	0.51	0.52	0.63	0.80	0.92
	RMSE [m]	14.3	14.9	12.6	10.1	7.9	7.0
	SNR_2[dB]	—	−19.8	4.7	9.7	17.7	19.7
150	PD	0.53	0.48	0.45	0.49	0.61	0.79
	RMSE [m]	29.8	31.4	31.1	28.1	23.3	19.9
	SNR_2[dB]	—	−24.1	0.4	5.4	10.4	15.4

V. Conclusion

In this letter, we have used an active RIS to get a second observation of the region inspected by a monostatic radar equipped with a digital array. We have designed the array gain factor of the radar transmitter and the RIS to uniformly cover the inspected region and solved the target detection and localization problem via a generalized likelihood ratio test. The numerical analysis shows that, for the same power budget, the active RIS improves the radar performance if a sufficiently large amplification gain can be guaranteed. Future studies should account for the clutter presence and should investigate the radar and RIS scanning policy when multiple regions need to be inspected, each one possibly containing multiple targets.

REFERENCES

[1] J. Huang and J. A. Encinar, *Reflectarray Antennas*. Hoboken, NJ, USA: Wiley, 2007.

[2] S. V. Hum and J. Perruisseau-Carrier, "Reconfigurable reflectarrays and array lenses for dynamic antenna beam control: A review," *IEEE Trans. Antennas Propag.*, vol. 62, no. 1, pp. 183–198, Jan. 2014.

[3] P. Nayeri, F. Yang, and A. Z. Elsherbeni, "Beam-scanning reflectarray antennas: A technical overview and state of the art," *IEEE Antennas Propag. Mag.*, vol. 57, no. 4, pp. 32–47, Aug. 2015.

[4] Q. He, S. Sun, and L. Zhou, "Tunable/reconfigurable metasurfaces: Physics and applications," *Research*, vol. 2019, 2019, Art. no. 1849272.

[5] O. Tsilipakos et al., "Toward intelligent metasurfaces: The progress from globally tunable metasurfaces to software-defined metasurfaces with an embedded network of controllers," *Adv. Opt. Mater.*, vol. 8, no. 17, 2020, Art. no. 2000783.

[6] R. Long, Y.-C. Liang, Y. Pei, and E. G. Larsson, "Active reconfigurable intelligent surface-aided wireless communications," *IEEE Trans. Wireless Commun.*, vol. 20, no. 8, pp. 4962–4975, Aug. 2021.

[7] K. Liu, Z. Zhang, L. Dai, S. Xu, and F. Yang, "Active reconfigurable intelligent surface: Fully-connected or sub-connected?," *IEEE Commun. Lett.*, vol. 26, no. 1, pp. 167–171, Jan. 2022.

[8] Z. Zhang et al., "Active RIS vs. passive RIS: Which will prevail in 6G?," *IEEE Trans. Commun.*, vol. 71, no. 3, pp. 1707–1725, Mar. 2023.

[9] Y. Liu et al., "Reconfigurable intelligent surfaces: Principles and opportunities," *IEEE Commun. Surveys Tuts.*, vol. 2, no. 3, pp. 1546–1577, Thirdquarter 2021.

[10] E. Björnson, H. Wymeersch, B. Matthiesen, P. Popovski, L. Sanguinetti, and E. de Carvalho, "Reconfigurable intelligent surfaces: A signal processing perspective with wireless applications," *IEEE Signal Process. Mag.*, vol. 39, no. 2, pp. 135–158, Mar. 2022.

[11] Q. Wu and R. Zhang, "Joint active and passive beamforming optimization for intelligent reflecting surface assisted SWIPT under QoS constraints," *IEEE J. Sel. Areas Commun.*, vol. 38, no. 8, pp. 1735–1748, Aug. 2020.

[12] C. Pan et al., "Intelligent reflecting surface aided MIMO broadcasting for simultaneous wireless information and power transfer," *IEEE J. Sel. Areas Commun.*, vol. 38, no. 8, pp. 1719–1734, Aug. 2020.

[13] C. Pan et al., "Multicell MIMO communications relying on intelligent reflecting surfaces," *IEEE Trans. Wireless Commun.*, vol. 19, no. 8, pp. 5218–5233, Aug. 2020.

[14] W. Tang et al., "MIMO transmission through reconfigurable intelligent surface: System design, analysis, and implementation," *IEEE J. Sel. Areas Commun.*, vol. 38, no. 11, pp. 2683–2699, Nov. 2020.

[15] Y.-C. Liang, Q. Zhang, J. Wang, R. Long, H. Zhou, and G. Yang, "Backscatter communication assisted by reconfigurable intelligent surfaces," *Proc. IEEE*, vol. 110, no. 9, pp. 1339–1357, Sep. 2022.

[16] H. Wymeersch, J. He, B. Denis, A. Clemente, and M. Juntti, "Radio localization and mapping with reconfigurable intelligent surfaces: Challenges, opportunities, and research directions," *IEEE Veh. Technol. Mag.*, vol. 15, no. 4, pp. 52–61, Dec. 2020.

[17] S. Buzzi, E. Grossi, M. Lops, and L. Venturino, "Radar target detection aided by reconfigurable intelligent surfaces," *IEEE Signal Process. Lett.*, vol. 28, pp. 1315–1319, 2021.

[18] A. Aubry, A. De Maio, and M. Rosamilia, "Reconfigurable intelligent surfaces for N-LOS radar surveillance," *IEEE Trans. Veh. Technol.*, vol. 70, no. 10, pp. 10735–10749, Oct. 2021.

[19] S. Buzzi, E. Grossi, M. Lops, and L. Venturino, "Foundations of MIMO radar detection aided by reconfigurable intelligent surfaces," *IEEE Trans. Signal Process.*, vol. 70, pp. 1749–1763, 2022.

[20] H. Zhang, H. Zhang, B. Di, K. Bian, Z. Han, and L. Song, "MetaRadar: Multi-target detection for reconfigurable intelligent surface aided radar systems," *IEEE Trans. Wireless Commun.*, vol. 21, no. 9, pp. 6994–7010, Sep. 2022.

[21] M. Rihan, E. Grossi, L. Venturino, and S. Buzzi, "Spatial diversity in radar detection via active reconfigurable intelligent surfaces," *IEEE Signal Process. Lett.*, vol. 29, pp. 1242–1246, 2022.

[22] J. Lee, J. Lee, and K. Yang, "Reflection-type RTD low-power amplifier with deep sub-mW DC power consumption," *IEEE Microw. Wireless Compon. Lett.*, vol. 24, no. 8, pp. 551–553, Aug. 2014.

[23] J. Lee and K. Yang, "RF power analysis on 5.8 GHz low-power amplifier using resonant tunneling diodes," *IEEE Microw. Wireless Compon. Lett.*, vol. 27, no. 1, pp. 61–63, Jan. 2017.

[24] F. Amato, C. W. Peterson, B. P. Degnan, and G. D. Durgin, "Tunneling RFID tags for long-range and low-power microwave applications," *IEEE J. Radio Freq. Identif.*, vol. 2, no. 2, pp. 93–103, Jun. 2018.

[25] J. Rao, Y. Zhang, S. Tang, Z. Li, C.-Y. Chiu, and R. Murch, "An active reconfigurable intelligent surface utilizing phase-reconfigurable reflection amplifiers," *IEEE Trans. Microw. Theory Techn.*, vol. 71, no. 7, pp. 3189–3202, Jul. 2023.

[26] M. Iwamura, H. Takahashi, and S. Nagata, "Relay technology in LTE-advanced," *NTT DOCOMO Techical J.*, vol. 12, no. 2, pp. 29–36, 2022.

[27] H. Guo et al., "A comparison between network-controlled repeaters and reconfigurable intelligent surfaces," 2022, *arXiv:2211.06974*.

[28] G. Leone, E. Moro, I. Filippini, A. Capone, and D. De Donno, "Towards reliable mmWave 6G RAN: Reconfigurable surfaces, smart repeaters, or both?," in *Proc. IEEE 20th Int. Symp. Model. Optim. Mobile, Ad hoc, Wireless Netw.*, 2022, pp. 81–88.

[29] R. A. Ayoubi, M. Mizmizi, D. Tagliaferri, D. De Donno, and U. Spagnolini, "Network-controlled repeaters vs. reconfigurable intelligent surfaces for 6G mmW coverage extension: A simulative comparison," in *Proc. IEEE 21st Mediterranean Commun. Comput. Netw. Conf.*, 2023, pp. 196–202.

[30] H. L. Van Trees, *Detection, Estimation, and Modulation Theory, Part IV: Optimum Array Processing*. New York, NY, USA: Wiley, 2002.

[31] M. A. Richards, *Fundamentals of Radar Signal Processing*, 2nd ed. New York, NY, USA: McGraw-Hill, 2005.

[32] M. I. Skolnik, *Introduction to Radar Systems*, 3rd ed. New York, NY, USA: McGraw-Hill, 2015.

[33] J. Joung, C. K. Ho, K. Adachi, and S. Sun, "A survey on power-amplifier-centric techniques for spectrum- and energy-efficient wireless communications," *IEEE Commun. Surveys Tuts.*, vol. 17, no. 1, pp. 315–333, Firstquarter 2015.

[34] H. L. Van Trees, *Detection, Estimation, and Modulation Theory, Part I: Detection, Estimation, and Linear Modulation Theory*. New York, NY, USA: Wiley, 2001.

[35] E. Grossi, M. Lops, A. M. Tulino, and L. Venturino, "Opportunistic sensing using mmWave communication signals: A subspace approach," *IEEE Trans. Wireless Commun.*, vol. 20, no. 7, pp. 4420–4434, Jul. 2021.

Open Access funding provided by 'Università degli Studi di Cassino e del Lazio Meridionale' within the CRUI CARE Agreement